Quantitative properties and receptor reserve of the IP_3 and calcium branch of G_q-coupled receptor signaling

Eamonn J. Dickson,[1] Björn H. Falkenburger,[1,2] and Bertil Hille[1]

[1]Department of Physiology and Biophysics, University of Washington, Seattle, WA 98195
[2]Department of Neurology, RWTH Aachen University, 52074 Aachen, Germany

G_q-coupled plasma membrane receptors activate phospholipase C (PLC), which hydrolyzes membrane phosphatidylinositol 4,5-bisphosphate (PIP_2) into the second messengers inositol 1,4,5-trisphosphate (IP_3) and diacylglycerol (DAG). This leads to calcium release, protein kinase C (PKC) activation, and sometimes PIP_2 depletion. To understand mechanisms governing these diverging signals and to determine which of these signals is responsible for the inhibition of KCNQ2/3 (K_V7.2/7.3) potassium channels, we monitored levels of PIP_2, IP_3, and calcium in single living cells. DAG and PKC are monitored in our companion paper (Falkenburger et al. 2013. *J. Gen. Physiol.* http://dx.doi.org/10.1085/jgp.201210887). The results extend our previous kinetic model of G_q-coupled receptor signaling to IP_3 and calcium. We find that activation of low-abundance endogenous $P2Y_2$ receptors by a saturating concentration of uridine 5′-triphosphate (UTP; 100 µM) leads to calcium release but not to PIP_2 depletion. Activation of overexpressed M_1 muscarinic receptors by 10 µM Oxo-M leads to a similar calcium release but also depletes PIP_2. KCNQ2/3 channels are inhibited by Oxo-M (by 85%), but not by UTP (<1%). These differences can be attributed purely to differences in receptor abundance. Full amplitude calcium responses can be elicited even after PIP_2 was partially depleted by overexpressed inducible phosphatidylinositol 5-phosphatases, suggesting that very low amounts of IP_3 suffice to elicit a full calcium release. Hence, weak PLC activation can elicit robust calcium signals without net PIP_2 depletion or KCNQ2/3 channel inhibition.

The Journal of General Physiology

INTRODUCTION

This and our companion paper in this issue (Falkenburger et al.) concern quantitative properties of signaling by seven-transmembrane receptors of the plasma membrane coupling to G_q ("G_qPCR"), which are examined experimentally and interpreted by kinetic modeling. Originally motivating this work was our long-standing interest in the regulation of the KCNQ2/3 potassium ion channel through activation of G_qPCRs. These receptors mediate diverse, important responses of neuronal and nonneuronal cells to stimuli such as light sensation in *Drosophila melanogaster* photoreceptors, contraction of vascular myocytes in response to adrenaline, behavioral and mood regulation in response to serotonin and dopamine, the effects of cholinergic drugs treating Alzheimer's disease, and the inhibition of KCNQ2/3 (K_V7.2/7.3) potassium channels.

G_q activates PLC, which cleaves the plasma membrane phospholipid phosphatidylinositol 4,5-bisphosphate (PIP_2) into the cytosolic messenger inositol 1,4,5-trisphosphate (IP_3) and membrane-bound diacylglycerol (DAG). IP_3 binding to IP_3 receptors (IP_3Rs) at the ER triggers the release of calcium into the cytosol. Calcium and DAG activate PKC. In addition, PLC may deplete its substrate, PIP_2, which is an activating cofactor for many ion channels and other membrane proteins (Suh and Hille, 2008; Logothetis et al., 2010). We explore all these actions here.

Intriguingly, the consequences of PIP_2 hydrolysis—(a) calcium release, (b) PKC activation, (c) net PIP_2 depletion, and (d) channel inhibition—do not always occur together. Moreover, most cells harbor several different kinds of receptors coupled to G_q, whose signaling responses sometimes differ. For example, in sympathetic neurons, bradykinin (through B_2 receptors) and acetylcholine (through M_1 muscarinic receptors [M_1Rs]) stimulate production of DAG, but only bradykinin leads to calcium release (Delmas and Brown, 2002), and only acetylcholine leads to observable PIP_2 depletion (Zaika et al., 2011). The existence of signaling microdomains and the calcium-induced acceleration of PIP_2 synthesis have been identified as factors contributing to this dissociation in sympathetic neurons (Delmas and Brown, 2002; Zaika et al., 2011).

E.J. Dickson and B.H. Falkenburger contributed equally to this paper.
Correspondence to Bertil Hille: hille@u.washington.edu

Abbreviations used in this paper: DAG, diacylglycerol; FRET, Förster resonance energy transfer; FRETr, FRET ratio; G_qPCR, G_q protein–coupled receptor; IP_3, inositol 1,4,5-trisphosphate; IP_3R, IP_3 receptor; M_1R, muscarinic receptor; Oxo-M, oxotremorine-M; $P2Y_2$R, purinergic receptor $P2Y_2$; PH, pleckstrin homology; PIP_2, phosphatidylinositol 4,5-bisphosphate; siRNA, small interfering RNA; SOCE, store-operated calcium entry; UTP, uridine 5′-triphosphate; VSP, voltage-sensitive 5-phosphatase.

© 2013 Dickson et al. This article is distributed under the terms of an Attribution–Noncommercial–Share Alike–No Mirror Sites license for the first six months after the publication date (see http://www.rupress.org/terms). After six months it is available under a Creative Commons License (Attribution–Noncommercial–Share Alike 3.0 Unported license, as described at http://creativecommons.org/licenses/by-nc-sa/3.0/).

The Rockefeller University Press $30.00
J. Gen. Physiol. Vol. 141 No. 5 521–535
www.jgp.org/cgi/doi/10.1085/jgp.201210886

We believe that knowing the quantitative requirements for PKC activation, calcium response, and PIP_2 depletion will be valuable for understanding how such signaling specificity can work, how PLC activation can lead to calcium release but not PIP_2 depletion, and how the effects of PLC activation through M_1R can differ from those of PLC activation through other G_qPCRs. Therefore, we performed a quantitative analysis of signaling events downstream of PLC, using fluorescent reporters for PIP_2, IP_3, and calcium, and in Falkenburger et al. (2013) for DAG and PKC. In that paper, these measurements are then used to extend a kinetic model of PLC signaling that builds on earlier versions (Horowitz et al., 2005; Falkenburger et al., 2010a,b). We show, for instance, that the requirements for calcium release and KCNQ2/3 channel inhibition are quite different: calcium release can be evoked with a far lower density of activated receptors.

MATERIALS AND METHODS

Cell culture and plasmids

tsA-201 cells were cultured in DMEM (Gibco) with 10% serum and 0.2% penicillin/streptomycin and passaged every 5 d. Cells were transiently transfected at ∼75% confluency with Lipofectamine 2000 (10 µl for a 3-cm dish; Invitrogen) and 0.5–1.2 µg DNA per plasmid. Cells were transfected 1 or 2 d before photometry experiments and 2 d before patch-clamp experiments. Cells were plated on polylysine-coated glass chips 12 h before experimentation.

The following plasmids were used: dark (nonfluorescent) and eYFP-labeled mouse M_1R (M_1R and M_1R-YFP; provided by N. Nathanson, University of Washington, Seattle, WA); human purinergic receptor $P2Y_2$ ($P2Y_2R$; The Missouri S&T cDNA Resource Center); EPAC1 (exchange protein directly activated by cAMP) Förster resonance energy transfer (FRET) probe for cAMP (provided by M. Lohse, University of Würzburg, Würzburg, Germany); human KCNQ2 (provided by D. McKinnon, State University of New York, Stony Brook, NY); human KCNQ3 (provided by T. Jentsch, Leibniz-Institut für Molekulare Pharmakologie, Berlin, Germany); eCFP-PH(PLCδ1), eYFP-PH(PLCδ1), and CFP-CAAX (from K-Ras; provided by K. Jalink, The Netherlands Cancer Institute, Amsterdam, Netherlands); the zebrafish voltage-sensitive phosphatase Dr-VSP-IRES-GFP (Dr-VSP; provided by Y. Okamura, Osaka University, Osaka, Japan); "Dark" Dr-VSP (Falkenburger et al., 2010b); and the IP_3 reporters IRIS-1 (provided by K. Mikoshiba, Institute of Physical and Chemical Research Brain Science Institute, Wako, Japan) and LIBRA version III (LIBRAvIII; provided by A. Tanimura, Health Sciences University of Hokkaido, Tobetsu, Japan). IRIS-1 is cytosolic, whereas LIBRAvIII is membrane localized by palmitoylation (membrane-targeting sequence of GAP43). Version III of LIBRA has the pH-stable YFP mutant Venus instead of eYFP and derives from rat IP_3R type III. The small interfering RNA (siRNA) for $P2Y_2$ was purchased from Santa Cruz Biotechnology, Inc. Membrane-targeted FRB (LDR) and CFP-FKBP-Inp54p were generated by T. Inoue (Johns Hopkins University, Baltimore, MD) and described previously (Suh et al., 2006). Hereafter, we refer to fluorophores simply as "CFP" or "YFP" regardless of whether regular or enhanced fluorescent proteins were used.

Electrophysiology

KCNQ2/3 currents were recorded in whole-cell gigaseal voltage-clamp or perforated-patch configuration using borosilicate glass pipettes with a resistance around 2.2 MΩ. Internal solution was (mM): 175 KCl, 5 $MgCl_2$, 5 HEPES, 0.1 K_4BAPTA, 3 Na_2ATP, and 0.1 Na_3GTP, pH 7.4 (KOH). Recordings used an EPC9 amplifier with Patchmaster 2.35 software (HEKA). Currents were filtered at 2.9 kHz. Sample intervals were 200 µs or slower. Series resistance was compensated by 70% after compensation of fast and slow capacitance. Leak was not subtracted. Holding potential was −60 mV. KCNQ2/3 current was quantified by measuring tail currents. Every 2 s, the membrane was depolarized to −20 mV for 400 ms and repolarized to −60 mV. KCNQ2/3 current activates slowly upon depolarization and deactivates slowly upon repolarization (see Fig. 1 A, bottom right). KCNQ2/3 tail currents were measured by comparing current at 20 and 400 ms after repolarization to −60 mV.

For perforated-patch recordings, amphotericin B was dissolved in DMSO on the day of recording (1 mg/10 µl), sonicated, diluted in internal solution to a working concentration of 300–500 µg/ml, and sonicated again. The tip of the patch pipette was filled with amphotericin B–free Ringer's solution by capillary action. After <5 min, access resistance was usually low enough to record KCNQ2/3 current.

Perfusion, extracellular buffer, and temperature

Cells were recorded in a 100-µl chamber continuously superfused (1 ml/min) with Ringer's solution containing (mM): 160 NaCl, 2.5 KCl, 2 $CaCl_2$, 1 $MgCl_2$, 10 HEPES, and 8 glucose, pH 7.4 (NaOH). All drugs were applied in the superfusate. As a measure of exchange time, when 2.5 mM KCl Ringer's solution was replaced by 30 mM KCl Ringer's solution (shifting the K^+ reversal potential positive of −60 mV), KCNQ2/3 tail currents were inverted with a delay of <1 s and a time constant of 2 s, which is sufficiently fast for the kinetics investigated here. All measurements reported in this paper were done at room temperature, 21–23°C.

Photometric calcium measurements

All optical measurements of calcium and FRET used a monochromatic light source (Polychrome IV; TILL Photonics) for epifluorescence illumination and one or two TILL photodiodes with suitable filters and dichroic mirrors for photometry. Photodiode voltages were acquired by Patchmaster (sampling 200 µs or slower), and after recording from each cell, an area of the coverslip without cells was measured as background. Cytosolic free calcium was measured with the low-affinity indicator Fura-4F (Invitrogen). For measurements without electrophysiology or in perforated-patch configuration, cell-permeable Fura-4F-AM ester was diluted to 2 µM in Ringer's solution supplemented with 0.2% pluoronic F-68. Cells were loaded for 40 min and then incubated in regular Ringer's solution for an additional 30 min to allow complete de-esterification of AM esters. For measurements in whole-cell configuration, 0.1 mM of cell-impermeable Fura-4F salt was added to the intracellular solution in the patch pipette. Fura-4F fluorescence was measured by stepping the excitation light to 340 nm for 100 ms and 380 nm for 20 ms every 4 s. (The recording time with 340-nm excitation was longer than for 380-nm excitation to compensate for the poorer signal-to-noise ratio with 340-nm excitation.) Excitation light was reflected by a 415-dclp or a three-color (89006bs; Chroma Technology Corp.) dichroic mirror. Fluorescence was detected using one photodiode with a 535/30-nm emission filter. Background fluorescence was subtracted, and the ratio of emission with 340-nm excitation (F_{340}) to emission with 380-nm excitation (F_{380}) was calculated offline using a custom macro for IGOR Pro 6.0 (WaveMetrics).

The following features were extracted from traces of Fura-4F ratio (F_{340}/F_{380}): baseline, mean ratio of the points preceding agonist application; peak, the maximum ratio reached within 20 s after agonist application; time to half-maximum, the delay between start of agonist application and the first time point where

the ratio exceeded 50% of the distance between baseline and peak; duration, the delay between time to half-maximum and the first time point when the ratio fell below 10% of the distance between baseline and peak. (The level of 10% was chosen to include a late "hump" or plateau of the Fura-4F signal in response to G_qPCR activation.)

Three methods for obtaining Fura-4F calibration curves were compared: (1) adding Fura-4F salt to solutions with known calcium concentrations and measuring droplets of these solutions, (2) measuring cells into which such solutions had been dialyzed by the whole-cell pipette, and (3) superfusing cells loaded with cell-permeable Fura-4F/AM with such solutions in the presence of 15 µM ionomycin. These calibrations yielded similar results. The calcium concentration corresponding to a given $r = F_{340}/F_{380}$ is given by: $[\text{calcium}] = K' (r - r_{min})/(r_{max} - r)$, where r_{min} is F_{340}/F_{380} with 20 mM EGTA and r_{max} is F_{340}/F_{380} with 2 mM calcium. Values of rmin and rmax were dependent on the dichroic mirror used in the microscope. The "triple dichroic" we used to measure FRET (89006bs; Chroma Technology Corp.) reflects short wavelength excitation light slightly less well than a dichroic mirror designed specifically for Fura measurements (DCLP 415). Accordingly, rmin and rmax were 0.017 and 0.245 for the 89006bs, and 0.050 and 0.737 for the DCLP 415. The calcium concentration at which the F340/F380 ratio change is half-maximal was $K' = 30$ µM, regardless of the dichroic used. 89006bs was used for experiments as in Fig. 7 C, and DCLP 415 was used in experiments as in Figs. 1 A, 2, 4, and 7 A.

We chose a low-affinity calcium indicator to better discriminate higher levels of cytosolic free calcium. Using such an indicator means that it is difficult to resolve low levels of resting calcium properly. It is for this reason that the figures show fura ratio F_{340}/F_{380}.

Photometric FRET measurements

Epifluorescence photometry measured FRET from CFP to YFP using a three-color dichroic mirror in the microscope, two photodiode detectors, and the excitation wavelength scanned in a ramp as described in Falkenburger et al. (2010b). Unless otherwise noted, sweeps were repeated every 2 s. The raw fluorescence data were corrected for background and for bleedthrough of CFP emission into the YFP recording channel, yielding the corrected fluorescence values CFP_C (480/40-nm emission with 440-nm excitation) and YFP_C (535/30-nm emission with 440-nm excitation). As before, FRET was expressed as the ratio $FRETr = YFP_C/CFP_C$. CFP_C, YFP_C, and FRETr are in arbitrary, apparatus-dependent units. In two panels as indicated, the points were mildly smoothed with a binomial filter that weighted immediate neighbors by a 0.25/0.5/0.25 algorithm.

For time courses of FRETr responses, we determined the following: baseline, mean FRETr of the points preceding agonist application; amplitude, the difference in FRETr between baseline and maximum or minimum for the response, the delay from agonist application to the onset of the response, and the exponential time constant of the rising and falling phases of the signal (by the fitting procedure of Jensen et al., 2009); and the duration at half-maximum.

Western blot

Cells were harvested in ice-cold PBS, centrifuged, and resuspended in 50 µl of lysis buffer (PBS with 1% Triton X-100, 1:100 EDTA, and protease inhibitor cocktail; Thermo Fisher Scientific). Lysates were incubated for 30 min on ice, triturating regularly. Lysates were cleared by centrifugation (13,000 *g* for 20 min at 4°C), and the supernatant was transferred to new tubes. 20 µg of protein was separated by SDS-PAGE using standard techniques (Falkenburger et al., 2010a). The primary antibody against human $P2Y_2$ (Santa Cruz Biotechnology, Inc.) was used at 1:500. The secondary antibody (1:30,000; goat anti–rabbit; Kirkegaard & Perry Laboratories, Inc.) was coupled to horseradish peroxidase and visualized by chemiluminescence using a digital imaging system (AlphaImager; AlphaInnotech). Bands were quantified by measuring the mean intensity in each lane with the same-sized region of interest. Results from four independent experiments were averaged for display. Results did not change when intensities for $P2Y_2$ were normalized to amounts of actin as a loading control.

Modeling

To summarize the results and test mechanistic hypotheses, a kinetic model of G_qPCR signaling was formulated and solved in the Virtual Cell simulation environment (University of Connecticut Health Center). Results of the model appear in many figures of this paper, but the rationale, design, and parameters of the model itself are described only in our companion paper (Falkenburger et al., 2013).

Statistics

Summarized data include one data point per cell. Numbers, bars, and markers represent mean ± SEM. The notation $n = xx$ refers to the number of cells averaged unless otherwise noted. Comparisons were made by one-way ANOVA and Tukey posthoc tests using GraphPad Prism software.

Online supplemental material

Fig. S1 shows that uridine 5′-triphosphate (UTP) does not inhibit KCNQ2/3 currents in whole-cell configuration. In Fig. S2, endogenous P2Y receptors change calcium but not cAMP. Fig. S3 shows expression patterns of FRET probes/pairs. Fig. S4 is a comparison of the IP_3 FRET probes LIBRAvIII versus IRIS-1. Fig. S5 shows modeling related to IP_3 and LIBRAvIII. In Fig. S6, time course of PIP_2 (PH-domain FRETr) during intermittent voltage-sensitive 5-phosphatase (VSP) activation is shown. Fig. S7 shows calcium rise in response to caffeine and ryanodine. Fig. S8 shows the origin of the plateau in the calcium and Fura-4F responses, and in Fig. S9, the time course of acceleration of PIP_2 synthesis is established. Figs. S1–S9 are available at http://www.jgp.org/cgi/content/full/jgp.201210886/DC1.

RESULTS

Activation of endogenous P2Y receptors evokes calcium release but not significant PIP_2 depletion

To gain insight into the IP_3 branch of signaling elicited by activation of G_qPCR and PLC, we monitored levels of PIP_2, IP_3, and calcium by optical probes and recorded KCNQ2/3 potassium currents in single living tsA-201 cells. The overall design was to compare responses with a purinergic agonist to those with a muscarinic agonist in cells transfected with M_1Rs. tsA-201 cells do not express endogenous M_1Rs. We previously measured both endogenous and overexpressed levels of components of the M_1R signaling cascade (Falkenburger et al., 2010a) and estimated the density of overexpressed M_1Rs as being several orders of magnitude higher (500–1,000 per μm^2) than typical estimates of endogenous receptors (1 per μm^2) such as endogenous purinergic receptors. Henceforward, we refer to transfected M_1Rs as "high-density" M_1Rs.

First, we measured calcium using Fura-4F. Despite the large expected difference in their receptor densities, we found that the Fura-4F response was similar when

we activated endogenous purinergic receptors using a saturating concentration of 100 µM UTP or activated high-density M_1Rs using 10 µM oxotremorine-M (Oxo-M; Fig. 1, A and B). In perforated-patch recording with either stimulus, the Fura-4F ratio (F_{340}/F_{380}) rose to values corresponding to ∼1–3 µM of free calcium. On average, the amplitude of the Fura-4F response to UTP was 98% of the Oxo-M response (Fig. 1 C), and the duration of the response (50–10% of maximum) was similar (Fig. 1 D). However, the UTP response did rise more slowly, taking approximately three times as long to reach half-maximal amplitude (Fig. 1 E), suggesting that the activation of G_q and PLC by UTP was less intense. The ambient resting calcium was below the threshold for reliable quantitation by the low-affinity Fura-4F dye.

When we recorded KCNQ2/3 potassium currents in the perforated-patch configuration simultaneously with Fura-4F signals, we were surprised to find that KCNQ2/3 currents were not inhibited by 100 µM UTP although they were inhibited by 10 µM Oxo-M (Fig. 1, A and F). The findings were similar in whole-cell configuration (Fig. S1, A and B), with <1% inhibition by UTP (22 cells) and 84% inhibition by Oxo-M (17 cells). Under the perforated-patch configuration, peak current was gradually growing (spontaneously) in some cells, sometimes leading to apparent "negative" values of inhibition by agonist. We show perforated-patch configuration in Fig. 1 because UTP did not elicit a calcium response in whole-cell configuration (Fig. S1, A and B). The absence of a whole-cell calcium response with UTP could be a consequence of (a) diffusion of IP_3 and calcium into the patch pipette, thereby reducing IP_3- and calcium-induced calcium release, and/or (b) an inhibitory effect of Mg^{2+} diffusion into the cell (Volpe et al., 1990).

The contrast between responses of P2Y receptors and M_1Rs thus raises a challenging question: How do two receptors produce a full-amplitude calcium signal, whereas only one of them inhibits KCNQ2/3 channels? To address this, we first identified the endogenous subtype of P2Y receptors in tsA-201 cells.

$P2Y_2R$ is the major endogenous G_qPCR responsible for UTP-activated calcium rises

tsA-201 cells express P2Y receptor subtypes 1, 2, 11, 12, and 14 (Atwood et al., 2011). Of these, only $P2Y_2R$ and $P2Y_{11}R$ are directly activated by UTP. Both use G_q as their primary transduction pathway, with $P2Y_{11}R$ also using G_s as a secondary transduction mechanism. We found that UTP does not produce a detectable change in cAMP levels as measured by a FRET sensor based on EPAC (Nikolaev et al., 2004; Fig. S2), suggesting that $P2Y_2R$ would more likely be the major endogenous receptor responsible for rises in cytosolic calcium. In the following experiments, we confirmed the expression and functional importance of $P2Y_2R$ in tsA-201 cells by (a) Western blot analysis, (b) testing the effects of a $P2Y_2R$ antagonist, and (c) $P2Y_2R$ "knockdown" by an established siRNA.

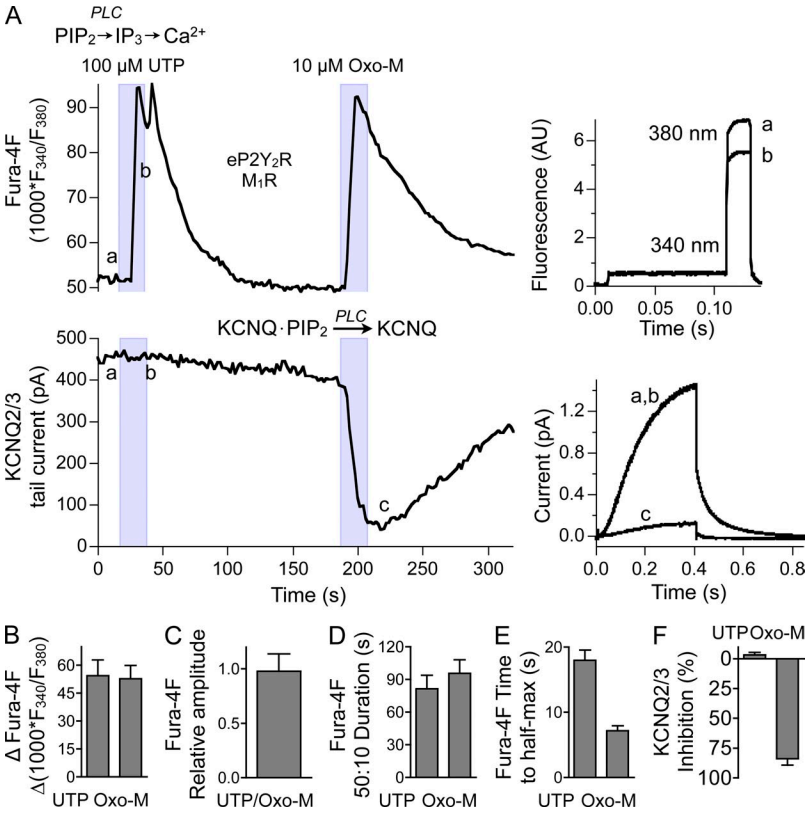

Figure 1. Activating endogenous purinergic receptors initiates a calcium rise but does not inhibit KCNQ2/3 current. tsA cells transfected with M_1R and KCNQ channel subunits were loaded with Fura4F-AM, fluorescence was recorded by photometry, and simultaneously, KCNQ2/3 potassium currents were recorded in perforated-patch configuration. (A; left) Time course of Fura-4F ratio and tail-current amplitudes. (Top right) Component single sweeps of data collection showing photodiode output as wavelength is stepped to 340 and 380 nm. (Bottom right) Depolarization-evoked KCNQ currents (steps from −60 to −20 mV for 400 ms). a, control; b, during exposure to 100 µM UTP; c, after exposure to 10 µM Oxo-M. eP2YP$_2$R, cells expressing endogenous P2Y$_2$Rs. (B) Summary of Fura-4F changes in response to UTP (n = 18) and Oxo-M (n = 15). (C) Ratio of peak Fura-4F changes elicited by UTP and Oxo-M in nine cells. (D) Duration from reaching half-maximal amplitude calcium response to the time point of falling below 10% of the amplitude (n as in B). (E) Summary of the time to half-maximal calcium response (n as in B). (F) KCNQ2/3 current inhibition in perforated-patch configuration by UTP (n = 9) and Oxo-M (n = 7).

Protein lysates from tsA-201 cells probed with a primary antibody against $P2Y_2R$ revealed two bands, one at a molecular mass of ~50 kD and the second at ~100 kD (Fig. 2 A). We assume that they represent receptor monomers (predicted protein M_r ~41 kD) and dimers. Lysates from populations of cells transfected with human $P2Y_2R$ showed greatly increased $P2Y_2R$ expression (both bands) and had to be diluted 100 times to produce bands of similar intensity to endogenous $P2Y_2R$. We conclude that on average, transient overexpression increases $P2Y_2R$ by 100-fold. Presumably it is increased even more than the 100-fold mean in some individual well-transfected cells (see Falkenburger et al., 2010a). Transfecting siRNA against $P2Y_2R$ decreased the intensity of the endogenous receptor bands by 90% (Fig. 2 A). The siRNA was also effective at reducing the augmented expression of transfected $P2Y_2R$ RNA (Fig. 2 A). Likewise, compared with control (Fig. 2 B), the $P2Y_2R$ siRNA decreased the peak amplitude of the UTP-evoked calcium rise by 90% in cells expressing only endogenous receptors, and it decreased the peak by 65% in $P2Y_2$-transfected cells (Fig. 2, C–E). 100 µM suramin, a $P2Y_2R$ antagonist, reduced the UTP-evoked calcium response by 68% (Fig. 2 F; $n = 5$). These separate lines of evidence indicate that the endogenous receptor activated by UTP is $P2Y_2$. Hereafter, we refer to endogenous $P2Y_2Rs$ as (low-density) "$eP2Y_2R$," and the combination of overexpressed and endogenous $P2Y_2Rs$ as (high-density) "$oP2Y_2R$".

High-density $P2Y_2R$ can evoke PIP_2 depletion and KCNQ2/3 current inhibition

To understand the apparent differences between $P2Y_2R$ and M_1R actions, we next compared their effects on plasma membrane PIP_2. The PIP_2 levels were monitored as FRET between fluorescently tagged PIP_2-binding pleckstrin homology (PH) domains from PLCδ$_1$ (van der Wal et al., 2001). Binding to PIP_2 at the plasma membrane brings CFP-PH and YFP-PH close enough together for FRET to occur. When PIP_2 is depleted, the PH domains translocate to the cytosol, and as the average distance between them increases, FRET decreases (Fig. 3 A). The first experiments compared high-density M_1R with low-density $eP2Y_2R$. Similar to our previous studies (Jensen et al., 2009; Falkenburger et al., 2010a), FRETr from the PH domain reporter of PIP_2 fell to ~50% of the initial value with the application of 10 µM Oxo-M (Fig. 3, B–D), indicating a strong depletion of PIP_2. In contrast, FRETr did not decrease significantly upon the application of 100 µM UTP (Fig. 3, B and D). Thus, we observed similar calcium responses to $eP2Y_2R$ and M_1R activation but saw PIP_2 depletion and KCNQ2/3 inhibition only with M_1R activation. We infer that the significant calcium rise observed with UTP neither suffices to induce net PIP_2 depletion (by, for example, activating PLCδ) nor to inhibit KCNQ2/3 current by itself.

Because of the difference in receptor densities between M_1R and $eP2Y_2R$, we hypothesized that a higher

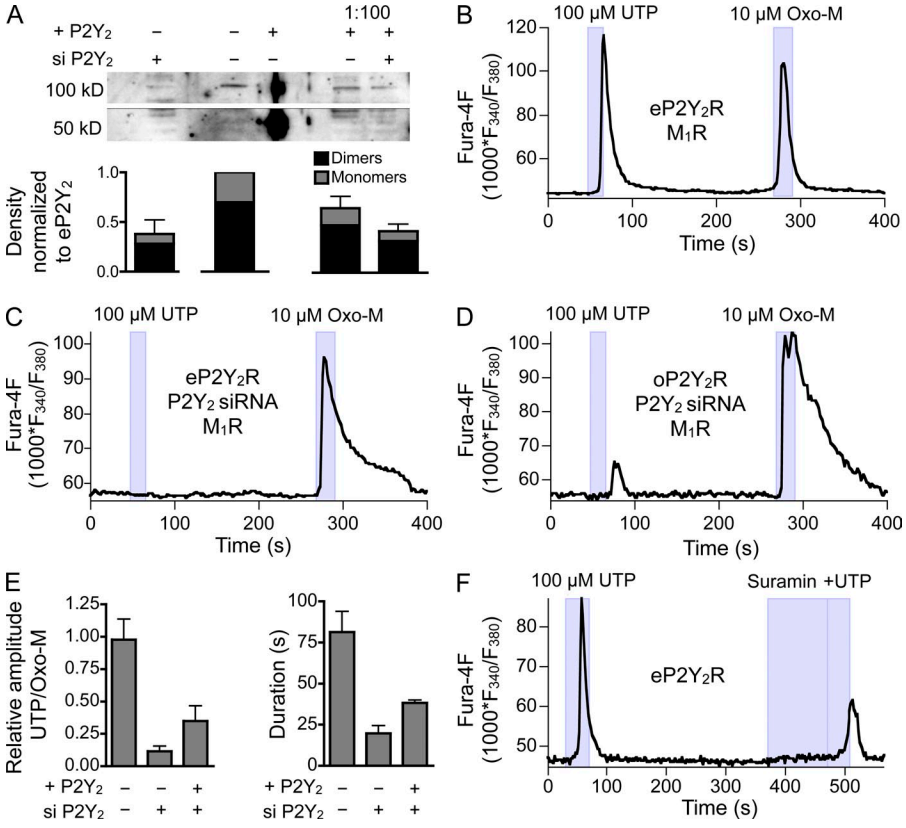

Figure 2. $P2Y_2$ is the endogenous receptor activated by UTP. (A; top) Western blot of lysates from untransfected cells, cells transfected with $P2Y_2$, and cells transfected with siRNA against $P2Y_2$. In the last two lanes, the lysate is diluted 100-fold. (Bottom) Summary of band densities normalized to the endogenous levels of $P2Y_2R$ from $n = 4$ experiments as in A. (B) Representative calcium responses to 100 µM UTP and 10 µM Oxo-M in a Fura-4F-AM–loaded cell without a patch pipette. (C) Representative calcium responses of a cell transfected with siRNA directed against the $eP2Y_2R$. (D) Representative calcium responses of a cell cotransfected with $hP2Y_2R$ and siRNA against $P2Y_2R$. (E) Summary of UTP-induced calcium responses after siRNA transfection ($n = 6$ for control, $n = 8$ for siRNA, and $n = 5$ for overexpression and siRNA). (F) Calcium responses in a cell exposed to the $P2Y_2R$ antagonist suramin (100 µM). Representative of $n = 7$ cells.

density of activated receptors is needed to deplete PIP_2 and to inhibit KCNQ2/3 currents than to induce calcium release. To test this hypothesis, we modified receptor density and receptor occupancy independently. First, we increased the total density of $P2Y_2R$ by overexpression, which, based on Western blot analysis, increased the density at least 100-fold (Fig. 2 A). In such cells with high-density $P2Y_2R$, 100 µM UTP did reduce PH domain FRETr (Fig. 3, C and D) and inhibit KCNQ2/3 current (Fig. 3, E and F) to a similar extent as Oxo-M acting through high-density M_1R. Second, we lowered the concentration of Oxo-M to reduce M_1R occupancy. Even a very low concentration of Oxo-M (1 nM) elicited a Fura-4F signal of similar size and duration as 10 µM Oxo-M (Fig. 4, A and B), although the time to half-maximum was longer with low Oxo-M concentrations. Previous work showed no reduction in PH-domain FRETr and no inhibition of KCNQ2/3 with 1 nM Oxo-M (Jensen et al., 2009). Thus, with high-density M_1Rs, more agonist is required to inhibit KCNQ2/3 and to deplete PIP_2 than to release calcium. In pharmacological terms, the 50% effective concentration for calcium release is much lower than that for KCNQ2/3 inhibition; i.e., the number of spare receptors, the receptor reserve, is large for calcium release and smaller for KCNQ2/3 inhibition and PIP_2 depletion.

These findings demonstrate that agonist and receptor requirements can differ between different outputs of G_q-coupled signaling and suggest the hypothesis that the differences we see between $P2Y_2R$ and M_1R actions might be explained entirely by a difference in receptor density. Our companion paper (Falkenburger et al., 2013) describes a mathematical, kinetic model based on this hypothesis that reproduces most of the features we have seen. Figs. 4 (C and D) and 5 (A and B) in this paper show simulations from that model. With appropriate choices of parameters, an increase in receptor density from 1 to 500 per μm^2 converts a response with little depletion of PIP_2 or decrease of current, yet still a strong Ca^{2+} rise and Fura-4F response (Fig. 5, A and B, "UTP"), into a response with the typical full Fura-4F signal, full inhibition of KCNQ current (Fig. 5 A, "Oxo-M"), strong Ca^{2+} increase, and full depletion of PIP_2 (Fig. 5 B, "Oxo-M"). The same calculations show that very low concentrations of agonist still evoke a full-amplitude Fura-4F response and a strong Ca^{2+} transient when receptor density is high (Fig. 4, C and D).

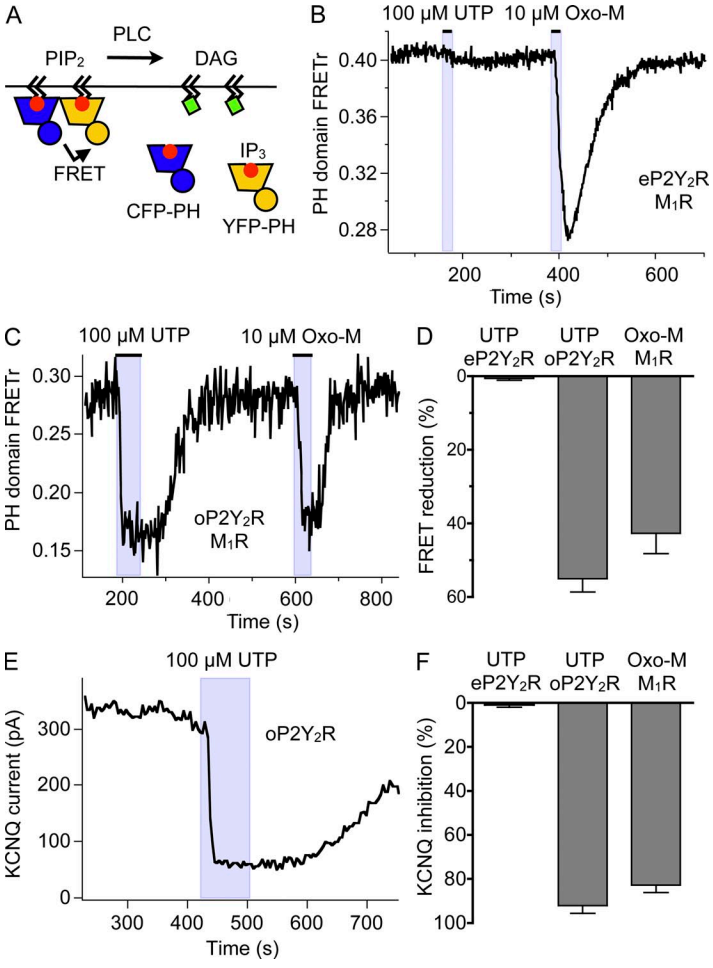

Figure 3. Activation of endogenous $P2Y_2R$ does not produce a net reduction in PIP_2. (A) Schematic representation of PIP_2 measurements by PH-domain FRET. Binding of PH-CFP and PH-YFP to PIP_2 at the plasma membrane brings CFP and YFP close enough together for FRET. After PIP_2 hydrolysis by PLC, PH-CFP and PH-YFP move apart into the cytosol. (B) FRETr time course from a single cell expressing PH-CFP and PH-YFP during exposure to 100 µM UTP and 10 µM Oxo-M. (C) FRETr time course from a cell expressing $hP2Y_2R$, M_1R, CFP-PH, and YFP-PH. (D) Summary of percent FRETr change in experiments like those in B and C ($n = 10$ with endogenous $P2Y_2$, $n = 12$ with high-density transfected $P2Y_2$, and $n = 13$ with high-density transfected M_1Rs). (E) Representative KCNQ2/3 tail-current changes with UTP in a cell transfected with KCNQ2, KCNQ3, and $P2Y_2R$. (F) Summary of KCNQ inhibition in experiments like those shown in E and Fig. 1 A ($n = 11$ for endogenous $P2Y_2$ and $n = 5$ for high-density $P2Y_2$).

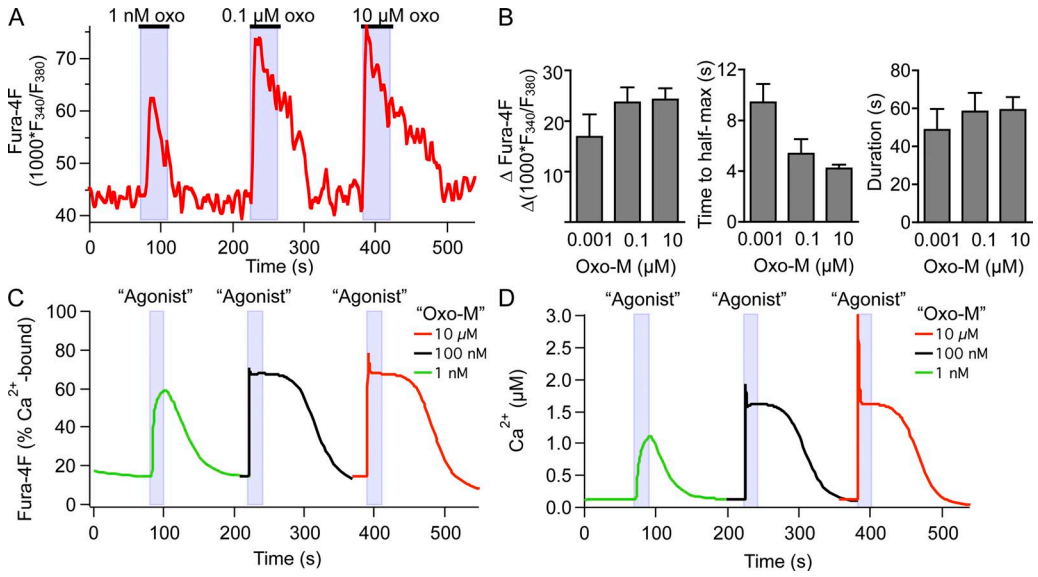

Figure 4. Similar calcium responses are evoked by low and high Oxo-M concentrations. (A) Representative calcium responses of a cell transfected with M_1Rs, loaded with Fura-4F-AM, and treated with 1 nM, 0.1 µM, or 10 µM Oxo-M. (B) Summary of Fura-4F amplitude, time to half-maximum, and duration for experiments as in A ($n = 16$). (C) Simulations from our kinetic model reproducing the observations in A. Quotation marks on Oxo-M are a reminder that this is a computer simulation rather than experiment. Assumed [Fura-4F] was 1 µM. (D) Simulation showing corresponding rises in cytosolic calcium concentration during 1 nM, 0.1 µM, and 10 µM Oxo-M. Fura-4F concentration was set at 0 µM.

Receptors stimulate IP_3 production

To identify at which stage of the G_q signaling cascade the receptor reserve arises, we measured IP_3 production in living tsA-201 cells using two FRET reporters, IRIS-1 (Matsu-ura et al., 2006) and LIBRAvIII (Tanimura et al., 2009). Both consist of CFP and YFP linked by the ligand-binding domain of the rat IP_3R type III. They show a reduction in FRET between CFP and YFP upon binding of IP_3. IRIS-1 is a cytosolic protein, whereas LIBRAvIII is targeted to the plasma membrane by a palmitoylation sequence from GAP43 (Fig. S3). The reported ligand concentrations for half-maximal FRET change are similar: 550 nM IP_3 for IRIS-1 and 490 nM for LIBRAvIII. These probes are insensitive to physiological changes of calcium. In our hands, IRIS-1 signals were difficult to interpret and were not graded with Oxo-M concentration. On average, the IRIS-1 response is an ~15% FRET decrease with invariant temporal characteristics in response to 1 nM, 100 nM, and 10 µM Oxo-M (Fig. S4, A and B, and not depicted). Further, with 10 µM Oxo-M, the delay before onset, the onset and recovery time constants, and the IRIS-1 response duration were longer than expected from our calcium measurements or from reported biochemical assays of IP_3 (Willars et al., 1998),

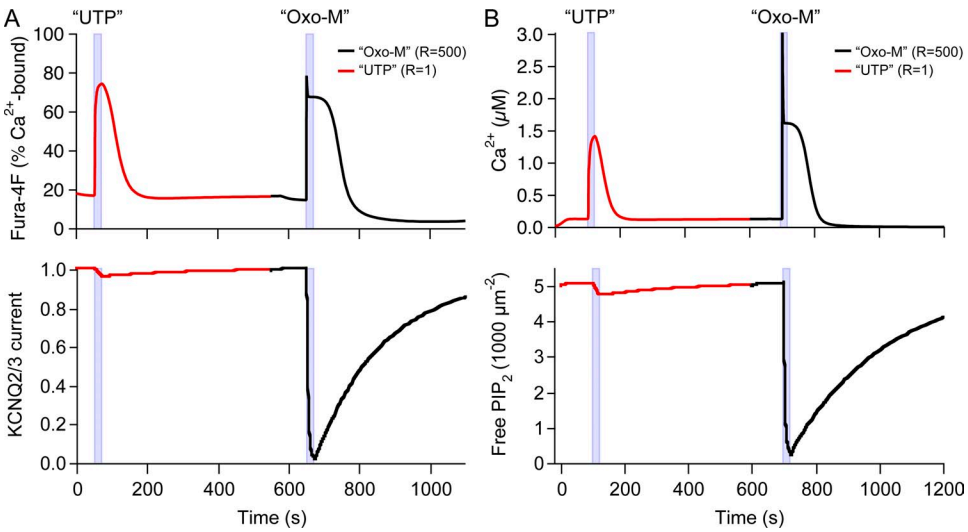

Figure 5. Receptor density can account for differences in calcium signaling and PIP_2 depletion. Simulations from our kinetic model. Low receptor densities (1 per µm^2) mimic ePY$_2$, and high receptor densities (500 per µm^2) mimic high-density M_1Rs. (A) Simulated time courses of Fura-4F (top) and KCNQ2/3 current (bottom) responses to UTP acting on low receptor densities (red line) and Oxo-M acting on high receptor densities (black line). [Fura-4F] was 1 µM. (B) Simulated time courses of calcium (top) and PIP_2 (bottom) concentration changes with low and high receptor densities. Fura-4F concentration was set at 0 µM.

and much longer than those observed with LIBRAvIII. Possible explanations for such unexpected kinetics include reporting of IP_3 in cellular regions far from the plasma membrane.

We therefore turned to membrane-localized LIBRAvIII. It responded to 10 µM Oxo-M with a small, reproducible FRETr decrease (Fig. 6 A). The IP_3 selectivity was assessed by overexpressing the enzyme IP_3 5-phosphatase, which can deplete IP_3 as fast as it is made in these cells (Horowitz et al., 2005). Overexpression of this enzyme eliminated the responses of LIBRAvIII (Fig. 6 A), confirming the FRET probe's selectivity for IP_3. We calibrated the probe by dialyzing different concentrations of IP_3 into the cell via a patch pipette (Fig. 6 B, circles). Time-dependent FRET changes began in <10 s after breakthrough. No detectable change in FRETr occurred with dialysis of 1 µM IP_3, whereas the response nearly saturated with dialysis of 10 µM IP_3. Thus, the LIBRAvIII probe has a fairly narrow dynamic range. To understand the dialysis protocol better, the entry of IP_3 was simulated by adding to our larger cell model a first-order exchange from the pipette through a rate-limiting orifice. This model reproduced the calibration experiment reasonably well (lines in Fig. 6 B), assuming a dissociation constant of 500 nM for the IP_3-LIBRA complex as reported by others (Tanimura et al., 2009). The model indicates that the endogenous steady-state IP_3 5-phosphatase activity, which allows a mean lifetime for IP_3 of only 12.5 s, severely reduces the cellular IP_3 during dialysis. Separate control experiments (not depicted) with fluorescent dyes in the pipette typically showed dialysis of dye into the cytosol with an exponential time constant of 50–70 s. With similar pipette exchange rates for IP_3 added to the model and retaining an active endogenous IP_3 phosphatase, the steady-state cytosolic IP_3 concentration reaches only roughly 20% of that in the pipette, and the time constant of the exponential change is only 20% of that with

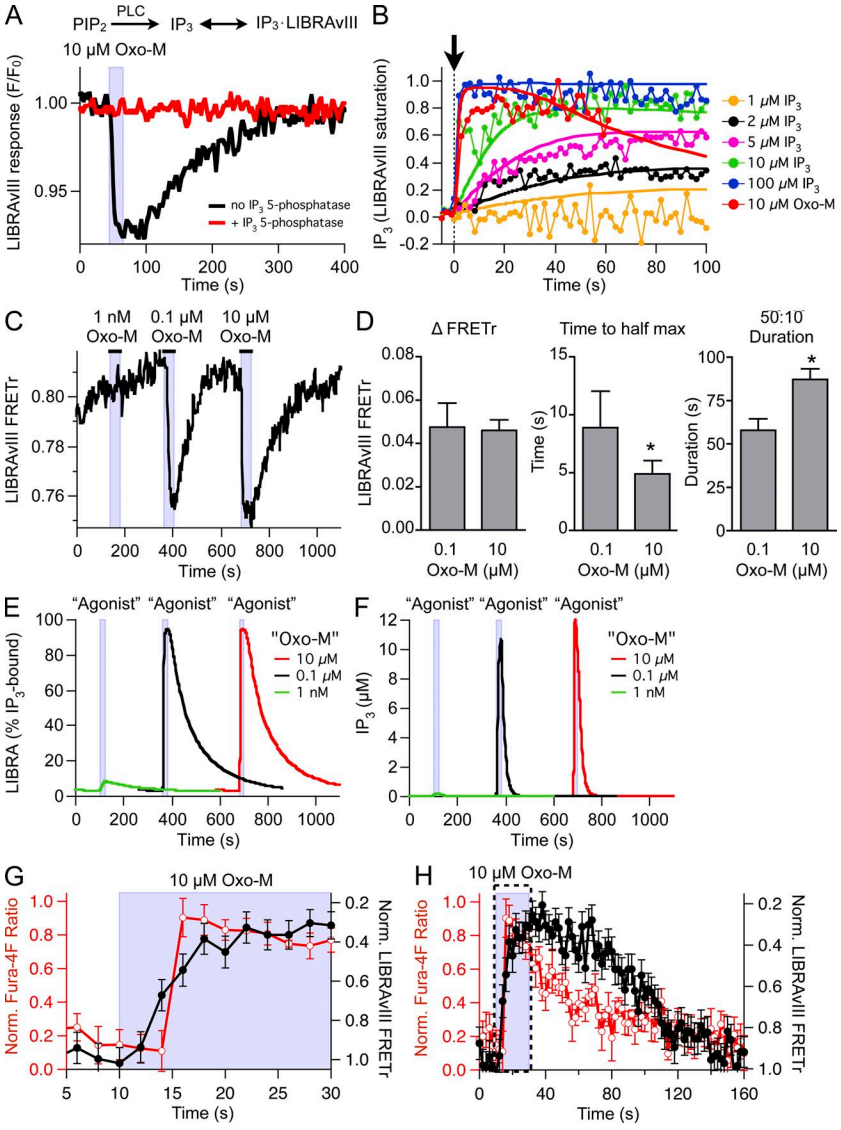

Figure 6. LIBRAvIII reports changes in IP_3 concentration before a rise in calcium. (A) Averaged time courses of normalized FRET from IP_3 probe LIBRAvIII in response to 10 µM Oxo-M. Cells were transfected with M_1R, LIBRAvIII, and with ($n = 6$) or without ($n = 7$) IP_3 5-phosphatase. Points were mildly filtered (see Materials and methods). (B) Calibration of LIBRAvIII. Cells were transfected with LIBRAvIII and patched with pipettes containing different concentrations of IP_3 (1–100 µM). Plasma membrane was ruptured at t = 0 s, leading to dialysis of IP_3 into the cytosol of the cell (lines with markers). A response to 10 µM Oxo-M is superimposed for comparison. Smooth curves without markers are model simulations of IP_3 entry assuming 6 µM of cytosolic LIBRAvIII, a dissociation constant for LIBRAvIII of 0.5 µM, and a 12.5-s lifetime for IP_3 in the cytosol (see Falkenburger et al., 2013 for details). (C) Representative FRET recording of a cell expressing LIBRAvIII and M_1R exposed to a series of increasing Oxo-M concentrations. Points were mildly filtered (see Materials and methods). (D) Summary of LIBRAvIII responses to 0.1 and 10 µM Oxo-M ($n = 7$). (E and F) Simulations showing the percentage of IP_3 bound to LIBRAvIII (E) and the concentration of IP_3 (F) after activation of M_1R (density, 500 per µm^2) with 1 nM, 100 nM, or 10 µm Oxo-M. [LIBRAvIII] was 6 µM for E and 0 µM for F. (G and H) Superimposed normalized experimental Fura-4F and LIBRAvIII responses to 10 µM Oxo-M ($n = 7$). G shows an expanded version of the dashed rectangle in H. Note that the scales for LIBRAvIII in G and H are inverted.

no cytosolic phosphatase (see Fig. S5 A). In addition LIBRAvIII significantly buffers the IP_3 (see Fig. S5 B).

LIBRAvIII responded to G_qPCR activation in a dose-dependent manner. No response was detected with 1 nM Oxo-M, whereas with 100 nM or 10 µM Oxo-M the amplitudes were not statistically different, which is consistent with the narrow dynamic range observed during IP_3 dialysis. However, the time courses differed (Fig. 6, C and D). Comparing responses to 100 nM versus 10 µM Oxo-M, the delay before onset was longer (18 ± 2 s vs. 9 ± 6 s), the onset slower (τ_{on} 7 ± 1 s vs. 3 ± 1 s), and the duration shorter (40 ± 3 s vs. 72 ± 10 s; Fig. 6 D). The slower response and faster recovery are expected from the weaker activation of PLC by 100 nM Oxo-M (Jensen et al., 2009).

What is the range of IP_3 changes? When the Oxo-M responses of LIBRAvIII were compared with those in the IP_3 calibration experiments, we found that 10 µM Oxo-M elicited responses similar in amplitude and kinetics to dialysis with 10 µM IP_3 in the pipette. The IP_3-binding curve of LIBRAvIII (Fig. S5 C) shows that LIBRAvIII does not discriminate well between IP_3 concentrations above 2 µM. We conclude that peak IP_3 is above 2 µM. The resting levels of IP_3 are below the level reached with 2 µM IP_3 in the pipette (<300 nM in the cell), which evoked a minimal FRETr decrease. Fig. 6 (E and F) shows that the dependence of the LIBRAvIII response amplitude, rise time, and duration on Oxo-M concentration was captured qualitatively in the kinetic model described in our companion paper (Falkenburger et al., 2013). In this model, free IP_3 rises to 10 µM in the absence of LIBRAvIII. This limit would result from cleavage of nearly all of the cellular PIP_2.

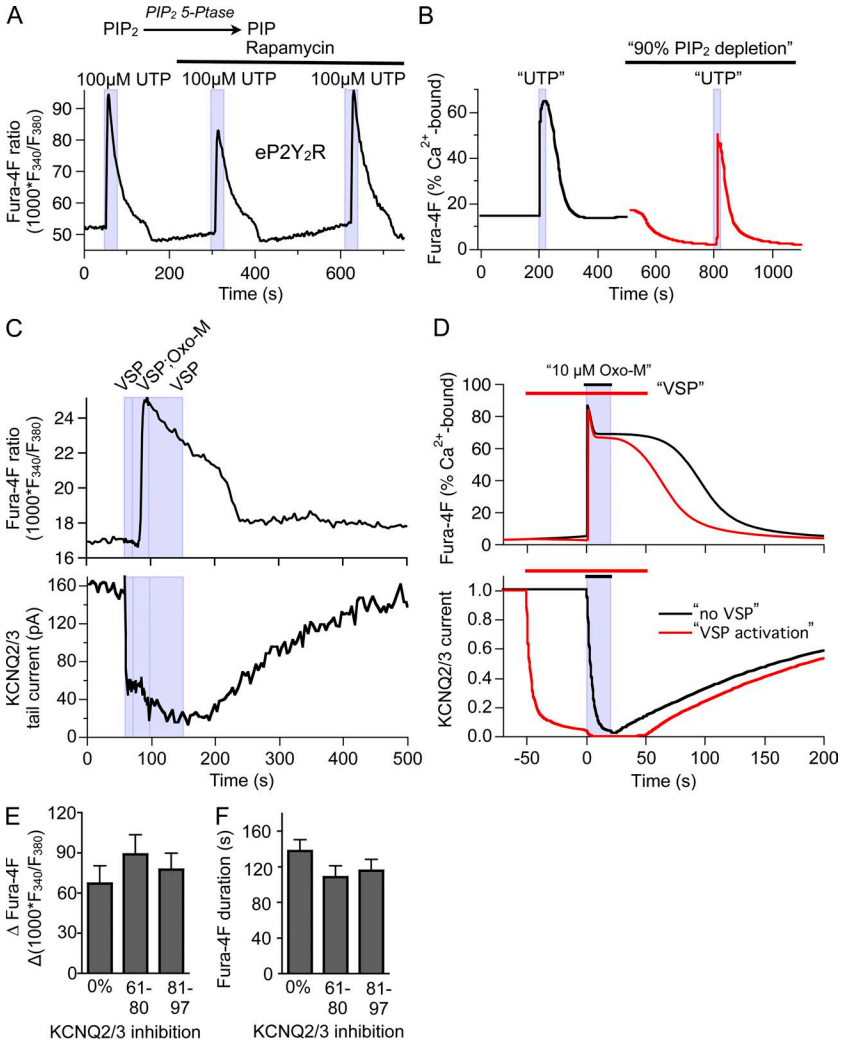

Figure 7. A little IP_3 suffices to initiate robust calcium signals. (A) Time course of calcium responses (Fura-4F) to UTP application. Cells were transfected with plasma membrane–targeted FRB and the PIP_2 5-phosphatase CFP-FKBP-Inp54p for recruitment of the 5-phosphatase to the plasma membrane by 5 µM rapamycin (bar). Representative of $n = 5$ cells. (B) Simulations from our kinetic model of the observations in A. A second calculation starts at 500 s in which a supplemental 5-phosphatase activity is turned on. Note that as PIP_2 gradually falls to a new steady state, less resting IP_3 is made by the basal PLC activity (a function of basal nucleotide exchange at Gα), and basal calcium release declines, slowly decreasing resting Fura-4F saturation. (C) Simultaneous recording of KCNQ2/3 tail current (bottom) and cytosolic calcium by Fura-4F ratio (top). Cells were transfected with M_1R, KCNQ2/3 channels, and the VSP. During baseline, KCNQ2/3 channels were activated maximally by depolarization from −60 to +40 mV for 200 ms every 600 ms. During the shaded rectangle marked "VSP," depolarization to +120 mV activated KCNQ2/3 channels as well as VSP, which depleted PIP_2 by ∼80% within seconds. Then, 10 µM Oxo-M was applied. The resulting calcium response was compared with calcium responses elicited before VSP-induced PIP_2 depletion. (D) Simulations showing Fura-4F saturation with calcium (top) and KCNQ2/3 current (bottom) in response to 10 µM Oxo-M at t = 0 s (black) and with activation of VSP from −50 s until 150 s (red). The extent of VSP activation was adjusted to have ∼90% KCNQ2/3 current inhibition (VSP_max = 0.3 s^{-1}). Note the reduction of the duration but not the amplitude of the Fura-4F signal by VSP. (E and F) Summary of experiments as in C. The recorded cells are grouped by extent of KCNQ2/3 inhibition (percent PIP_2 depletion) for summaries.

A low threshold for IP_3-dependent calcium release

We now turn to Ca^{2+} release from the ER. To learn the kinetic relation of IP_3 production to calcium release, we overlaid normalized experimental Fura-4F and LIBRAvIII responses for 10 µM Oxo-M (Fig. 6, G and H). LIBRAvIII reports a rise in IP_3 beginning already at 2 s, whereas the sudden upstroke of the Fura-4F signal occurs only between 4 and 6 s (Fig. 6 G). Hence, LIBRAvIII is a fast reporter of IP_3, and IP_3 production starts early. However, once initiated, the resulting calcium response rises more rapidly and peaks sooner than the IP_3 signal (Fig. 6 G). The Ca^{2+} rise, in particular its stereotypical amplitude and the concentration-dependent time to half-maximum (Fig. 4 B), is nearly like a regenerative response, rising abruptly with positive feedback when graded IP_3 accumulation reaches a certain level. The decay time courses for calcium and IP_3 are quite different (Fig. 6 H), reflecting their mechanistically separate clearance mechanisms.

Despite the strong Fura-4F signal produced by 1 nM Oxo-M (Fig. 4 A), the amount of IP_3 made at that low agonist concentration is too small to be reported by LIBRAvIII (Fig. 6 C). A minimal production of IP_3 suffices to initiate the calcium transient. This conclusion was reinforced by experiments showing little change of calcium responses upon reducing the available PIP_2 with coexpressed PIP_2 5-phosphatases. Such prior PIP_2 depletion ought to reduce the amount of IP_3 that can be produced by a given stimulus. First, we used rapamycin-induced dimerization of an FKBP domain with an FRB domain to "activate" the PIP_2 5-phosphatase Inp54p. When FKBP-tagged Inp54p is expressed together with plasma membrane–targeted FRB, the addition of rapamycin leads to translocation of the phosphatase to the plasma membrane and strong PIP_2 depletion (Suh et al., 2006). However, this manipulation did not reduce the amplitude of subsequent calcium responses to UTP (Fig. 7 A). The model also shows a resistance of the calcium response to 90% depletion of PIP_2 (Fig. 7 B). A second approach used a VSP to deplete PIP_2 and gave the same result (Fig. 7 C). Depolarization activates VSP reversibly and depletes plasma membrane PIP_2 (Murata and Okamura, 2007; Falkenburger et al., 2010b). PIP_2 levels were continuously monitored by recording KCNQ2/3 currents. To record KCNQ2/3 currents while keeping PIP_2 levels low over tens of seconds in VSP-transfected cells, we stepped cyclically from a holding potential of −60 to +120 mV for 400 ms, every 800 ms, and measured KCNQ2/3 tail currents at −60 mV. On average, the intermittent depolarization to +120 mV was sufficient to reduce KCNQ2/3 current by ∼80%. The time course of PIP_2 reduction as reported by PH-domain FRET was saw-toothed with an overall relaxation time constant of 10 s (Fig. S6). Despite this accumulating PIP_2 depletion, 10 µM Oxo-M could still evoke a full-amplitude calcium response (Fig. 7 C). Because the KCNQ2/3 current reduction achieved by the intermittent depolarization to +120 mV varied with VSP expression levels, we grouped the recorded cells by the extent of KCNQ2/3 inhibition for quantification (Fig. 7, E and F). Simulations from our kinetic model show that when VSP activity was adjusted to give a 90% reduction in KCNQ2/3 current, 10 µM Oxo-M generated a calcium response of similar amplitude but reduced duration (Fig. 7 D), similar to our experimental data (Fig. 7, E and F). In summary, activation of PLC can generate sufficient IP_3 for a calcium response even when PIP_2 levels are only a fraction of normal. It should be emphasized that the two 5-phosphatase treatments we used do lower PIP_2 considerably but never to zero because PIP_2 synthesis continues.

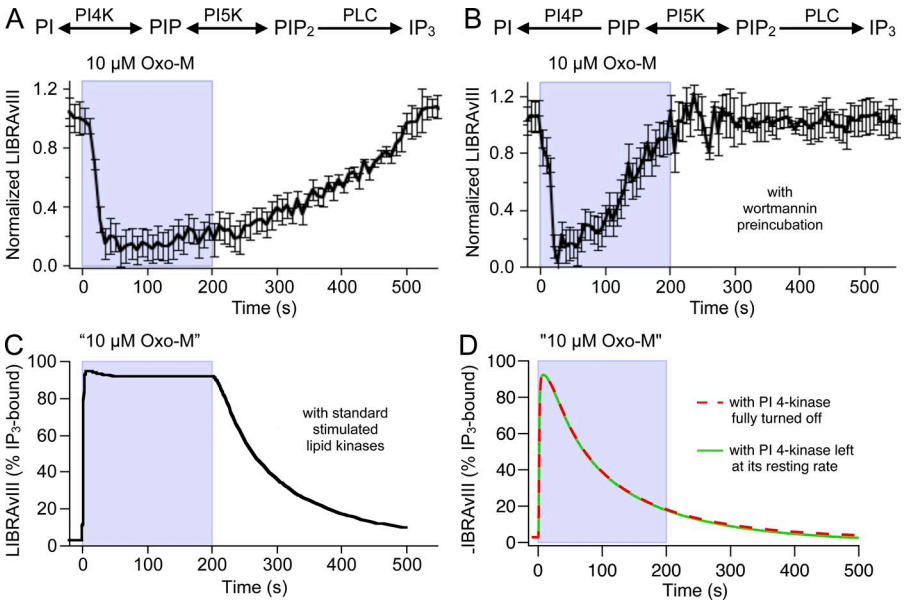

Figure 8. PIP_2 synthesis is required for maintained IP_3 production. To determine whether PIP_2 is synthesized during G_q activation, we inhibited PI 4-kinases by 30 µM wortmannin during a prolonged application of Oxo-M (200 s at 10 µM) and measured IP_3 production by LIBRAvIII. Cells were exposed to wortmannin for 5 min before start of recording. (A and B) Time course of normalized LIBRAvIII responses (control, $n = 8$ cells; wortmannin, $n = 5$). (C and D) Simulations from model. In C, the PI 4-kinase reaction was accelerated during agonist application with the "standard" time course shown in Fig. S9 A. In D, the PI 4-kinase was either left unchanged at its resting rate or turned off fully so that only the PIP_2 already present at rest is available to generate IP_3. To achieve a stable baseline with PI 4-kinase off, the PI 4-phosphatase reaction was turned off as well in this case.

Ongoing PIP_2 synthesis is required for continual IP_3 production

Is there significant synthesis of PIP_2 during agonist application? Throughout a 200-s application of 10 µM Oxo-M, IP_3 remained elevated, with some possible sag after an initial peak (Fig. 8 A). Given that (a) the lifetime of IP_3 is short (Fig. 6) and (b) PIP_2 is depleted by 90% during 10 µM Oxo-M (Horowitz et al., 2005), this continued production of IP_3 implies that new precursor PIP_2 is being formed as PLC is breaking it down. The rate-limiting step in PIP_2 synthesis is the PI 4-kinase activity; the PIP 5-kinase activity that makes PIP_2 from PI(4)P is 20 times faster (Falkenburger et al., 2010b). The slow step is probably accelerated during agonist application (Xu et al., 2003; Falkenburger et al., 2010b). To determine the importance of de novo PIP_2 synthesis during Oxo-M stimulation, we inhibited the PI 4-kinase using 30 µM wortmannin. After wortmannin, the initial amplitude of the LIBRAvIII FRETr response to Oxo-M was normal, but then it relaxed back to baseline while Oxo-M was still present (Fig. 8 B): IP_3 production had stopped. Fig. 8 (C and D) shows that a model with accelerated PIP_2 synthesis during Oxo-M application can explain maintained IP_3 elevation throughout Oxo-M application, and that continued IP_3 production fades if PI 4-kinase is not accelerated or is turned off fully.

DISCUSSION

To provide a more complete description of signaling by two different G_q-coupled receptors, we have performed quantitative kinetic measurements of PIP_2, IP_3, calcium, and KCNQ2/3 channel current in response to agonist application. Our measurements in tsA-201 cells show that (a) endogenous $P2Y_2$Rs activate the PLC pathway and signal to KCNQ channels much less effectively than M_1Rs expressed at high density; (b) experimentally, these differences are largely removed when $P2Y_2$Rs are expressed at high density; (c) very little IP_3 needs to be generated to induce a robust calcium release; (d) less receptor stimulation is needed to elicit a Ca^{2+} elevation than to deplete PIP_2 or to inhibit KCNQ channels; and (e) accelerated PIP_2 synthesis probably boosts IP_3 production during long receptor activation. These measurements further guided and are explained by an expanded kinetic model detailed in our companion paper (Falkenburger et al., 2013).

Differences between $P2Y_2$Rs and M_1Rs

We first revisit the contrasting actions of endogenous $P2Y_2$Rs and high-density M_1Rs. A saturating concentration of UTP acting on e$P2Y_2$Rs leads to calcium release without inhibition of KCNQ2/3 channels, whereas a saturating concentration of Oxo-M acting on high-density M_1Rs does both. Nevertheless, we conclude that there is no qualitative difference between $P2Y_2$R and M_1R actions. Our measurements show that endogenous $P2Y_2$Rs are at least 100-fold less abundant than overexpressed $P2Y_2$Rs, and our modeling shows that a 100–500-fold difference in receptor density between endogenous $P2Y_2$Rs and overexpressed M_1Rs is sufficient to explain all observations. In support, decreasing the number of activated M_1Rs by using an extremely low concentration of agonist (1 nM Oxo-M) mimics the responses to endogenous $P2Y_2$R activation by a saturating concentration of UTP. Conversely, increasing the number of $P2Y_2$Rs by overexpression makes the effects of UTP mimic those of Oxo-M. The density of endogenous purinergic receptors that we estimate is in a range expected from our previous estimate of endogenous G proteins and a typical ratio of G proteins to receptors (Falkenburger et al., 2010a). We therefore attribute the observed differences between UTP and Oxo-M primarily to a difference in receptor numbers. Such observations illustrate how quantitative differences in the abundance of a signaling component can result in apparent qualitative differences in responses.

Comparison with neurons

In sympathetic neurons, activation of M_1Rs leads to PIP_2 depletion (Zaika et al., 2011), and activation of B_2 receptors leads to calcium release (Delmas and Brown, 2002). Based on the findings described here, the first observation might be explained by a high density of M_1Rs and a low density of B_2 receptors in these neurons. Of course, receptors can be arranged in more interesting ways than just being high or low density, particularly in differentiated cells with specialized membrane compartments (e.g., spines, cilia, microvilli, or the apical membranes of epithelia). What counts for downstream effects is not the overall density of receptors but the local density "seen" by PLC molecules. Our data in tsA201 cells suggest that we do not need many PLC molecules (10 per μm^2) to fully deplete PIP_2 with the time course and concentration dependence observed experimentally. The interaction of signaling molecules will be strongly affected by inhomogenous densities resulting from membrane compartmentalization and scaffolding molecules. Nonetheless, we believe that the estimates for affinities and binding kinetics between M_1R, G_q, and PLC derived from our previous experiments and modeling (Jensen et al., 2009; Falkenburger et al., 2010a,b) are accurate and similarly apply to sympathetic neurons. Consequently, we have to assume at least 10 μm^{-2} molecules of PLC to deplete PIP_2 in sympathetic neurons and a density of M_1R that is high, at least in the vicinity of PLC.

It is not unexpected that low-density B_2 receptors can lead to calcium release, but it is hard to explain why M_1Rs do not. Others have suggested that B_2 receptors are close to IP_3Rs and M_1Rs are not, and that fast IP_3 degradation prevents its diffusion from M_1R-activated PLC to IP_3Rs (Delmas et al., 2004). Expanding measurements

and modeling into these spatial aspects will be an important next step to further understand how signaling specificity of GqPCR works.

Calcium signaling needs only minimal stimulation of PLC

Different signaling end points require different intensities of stimulation of receptors and PLC. For example, M_1R agonist binding has a midpoint of 4–10 µM for Oxo-M (Jensen et al., 2009), yet with high-density M_1R, closure of KCNQ2/3 channels and FRET interactions between $G\alpha_q$ and PLC and those between M_1R and G all have midpoints at 120–330 nM Oxo-M (Jensen et al., 2009). The release of stored calcium by IP_3 seems to be engaged by the smallest stimulation of receptors and PLC in our tsA cells: (a) Exposure to 1 nM Oxo-M activates PLC sufficiently to evoke a calcium rise, even though it produces too little IP_3 to be detected by the LIBRAvIII IP_3 reporter. (b) Calcium is released by activation of endogenous UTP receptors without a measurable net depletion of plasma membrane PIP_2. (c) A significant calcium release can be elicited even after depleting much of the normal PIP_2 using exogenous PIP_2 5-phosphatases, whether by rapamycin-induced protein dimerization or by VSP combined with membrane depolarization. These manipulations reduced PIP_2, and probably IP_3 production, by up to 90% as judged from KCNQ2/3 current inhibition. In drug discovery with overexpressed G_qPCRs, calcium measurements are often used as an assay for receptor activation. Such assays should give extremely sensitive responses. The release takes on a somewhat all-or-none character from regenerative positive feedback and occurs at the very low end of receptor occupancy (see below) rather than being broadly graded with receptor activation.

Several factors conspire to allow a small stimulus to make a strong calcium response and for the calcium response to be less graded as a function of agonist concentration. We use ideas from published experiments corroborated by our modeling (see Falkenburger et al., 2013) as an explanation. As is discussed in our companion paper, there are many observations of the IP_3 and calcium dependence of IP_3R channel opening. They all agree that both IP_3 and calcium show cooperativity, with channel activation following power law dependences (second-fourth power) of their concentrations that steepen the activation curve, as originally described by Bezprozvanny et al. (1991) and reviewed by Foskett et al. (2007). Calcium also activates PLC, thus accelerating IP_3 production. In our model, IP_3 turns on calcium release with as little as 1% full IP_3 production (which can rise as high as ∼12 µM IP_3 for the strongest activation). Half-maximal activation of channel opening by 100–300 nM Ca^{2+} is augmented by local microdomains of calcium rise around active groups of receptors. Finally, in real cells, but not part of our model, ryanodine receptors on the ER can also add to the Ca^{2+}-induced Ca^{2+} release. There are conflicting reports in the literature concerning ryanodine receptors, but our cells responded robustly with a calcium transient upon application of caffeine (Fig. S7), suggesting that tsA-201 cells do express ryanodine receptors and that a more complete model should include them. Hence, although the time course and duration of calcium signals is somewhat graded with stimulus intensity, the peak amplitude rises fairly abruptly, and the range over which the response amplitude is graded is compressed.

There are many published partial models of the IP_3R. The rationale for design and parameters of our model are detailed in our companion paper. We now consider how our model explains calcium transients in terms that are instructive but quite likely would differ in detail had we chosen another model of the IP_3R: The calcium response even to short applications of 10 µM Oxo-M is protracted in a late "hump" or plateau (Figs. 2, C and D, and 4 A). During longer Oxo-M applications (200 s), the response could be reduced and shortened by switching from 2 to 0 mM of extracellular calcium (see Fig. 9 in Horowitz et al., 2005), a standard test for store-operated calcium entry (SOCE). Our model does not include SOCE. Nevertheless, it does produce a plateau that prolongs the calcium response (Figs. 5 A and 8, B and C). This plateau results from unanticipated delayed and nonlinear effects of calcium binding to the IP_3R. In the model, >99.7% of the IP_3Rs become inactivated within the first second as a consequence of rising calcium (Fig. S8 A, $1\text{-}h^3$). Calcium is then gradually cleared through the SERCA pump, and as calcium falls again, a small percentage (0.1%) of receptors recover from inactivation by t = 20 s (while IP_3 is still high), producing a second phase of calcium flux in IP_3Rs. The resulting calcium plateau represents a dynamic steady state of calcium release and calcium clearance, and its height in our model is determined by the maximum transport capacity of the SERCA pump (vP; Fig. S8 B). The subsequent, final decrease in cytosolic calcium is caused by the fall in occupancy of IP_3-binding sites on the IP_3R that occurs with declining IP_3 levels. The duration of the calcium response is a function of the apparent affinity of the IP_3R for IP_3 and was determined primarily by the duration of the IP_3 elevation and by K_{IP3} (Fig. S8 C). We conclude that a plateau in the calcium response can result from intrinsic properties of the IP_3R and is not necessarily a sign of SOCE.

In pharmacological terms, there are spare receptors, a significant receptor reserve, for calcium signaling. Thus, according to our model, 1 nM Oxo-M would occupy only 0.06% of the overexpressed M_1Rs and activate only 0.3% of the endogenous PLC. As a consequence, 0.1% of the PIP_2 is hydrolyzed per second. In the absence of LIBRAvIII, cytosolic IP_3 would rise to 200 nM after 20 s. This amount is well above the half-activating

concentration for IP_3R calcium release yet below the 500-nM half-saturation concentration for detection by the lower-affinity LIBRAvIII reporter.

PIP_2 synthesis must be accelerated during G_qPCR activation

A couple of seconds after agonist addition, LIBRAvIII starts reporting an increase in IP_3, and the IP_3 elevation lasts throughout a 200-s agonist application despite the major decline of PIP_2 concentration and KCNQ currents. The IP_3 elevation requires continued PIP_2 synthesis, as it is not maintained after wortmannin treatment, which blocks type III PI 4-kinase. Similar persistent IP_3 production, sensitive to wortmannin, has been shown in experiments with radiolabeled inositol in SH-SY5Y cells (Nakanishi et al., 1995; Willars et al., 1998). Our standard kinetic model has resting rates for PI 4-kinase and PIP 5-kinase, chosen to match the recovery of PIP_2 both after depletion by PLC and after depletion by VSP (Horowitz et al., 2005; Falkenburger et al., 2010b). The 5-kinase is ∼20 times faster than the 4-kinase, making the wortmannin-sensitive PI 4-kinase the rate-limiting enzyme of PIP_2 synthesis. In the model, the mean lifetime of an IP_3 molecule is only 12.5 s, and we find that the chosen resting rates of PIP_2 synthesis are too slow to support the observed persistent IP_3 production during agonist application. These observations require that the rate of the PI 4-kinase be elevated temporarily during G_qPCR activation as was done in the model of Xu et al. (2003).

We have not studied the biochemical mechanism of kinase acceleration. There are several types of PI 4-kinase that synthesize PI(4)P. Shapiro and colleagues found that the inhibition of calcium currents in superior cervical ganglion cells by G_qPCR activation, which is attributed to PIP_2 depletion, is facilitated by dominant-negative neuronal calcium sensor 1 (NCS-1) (Gamper et al., 2004; Zaika et al., 2007, 2011). NCS-1 binds calcium and PI 4-kinase IIIβ (Zhao et al., 2001). In PC12 cells, overexpression of NCS-1 increased basal levels of PI(4)P and PI(4,5)P_2 and consequently G_qPCR-induced IP_3 production (Koizumi et al., 2002), suggesting a regulation of constitutive PIP_2 synthesis. The inhibition of receptor-induced responses by wortmannin (Nakanishi et al., 1995) suggests a type III PI 4-kinase, and indeed PIK93, a specific inhibitor of PI 4-kinase IIIβ, facilitated inhibition of calcium currents in superior cervical ganglion cells (Zaika et al., 2011). Yet, PIK93 did not affect IP_3 production by angiotensin or recovery of PI(4)P and PI(4,5)P_2 in HEK293 cells. Instead, PI(4,5)P_2 levels were most strongly depressed during angiotensin application in cells expressing siRNA for PI 4-kinase IIIα (Balla et al., 2008). Earlier studies had suggested that neither subtype is localized to the plasma membrane (Balla, 2007), but PI4-kinase IIIα was recently found to be targeted to the plasma membrane by a complex containing several additional proteins (Nakatsu et al., 2012). As an alternative to PI 4-kinase acceleration, PI(4)P supply might be accelerated during G_qPCR activation by increased delivery of PI(4)P to the plasma membrane, for instance, by vesicle trafficking or by the sterol transfer protein Osh4p (de Saint-Jean et al., 2011) from the Golgi.

There are also several types of PIP 5-kinases—1α, 1β, and 1γ—that synthesize PI(4,5)P_2. All are constitutively inhibited by phosphorylation. They are activated by phosphatidic acid, the product of DAG kinase (Kanaho et al., 2007), activated by the small GTPase RhoA (Oude Weernink et al., 2004), which can be stimulated by G_qPCR (Dutt et al., 2002), and activated by dephosphorylation through phosphatases that can be stimulated by calcium elevation (Unoki et al., 2012). Inhibition of Rho facilitated PIP_2 depletion during G_qPCR activation in superior cervical ganglion cells (Zaika et al., 2011). The PIP 5-kinase subtype involved in G_qPCR-induced synthesis appears to depend on the cell type (Tolias et al., 2000; Wang et al., 2004, 2008).

Although we do not know the biochemical mechanism, our model provides constraints for the time course of the acceleration of PIP_2 synthesis during G_qPCR activation. Assuming a very fast onset of acceleration in the model (red trace in Fig. S9 A) produced a transient increase in PIP_2 (red trace in Fig. S9 B), which we did not observe experimentally when recording KCNQ2/3 current. Therefore, onset may rise with a time constant of 1 s or longer after receptor activation (black traces in Fig. S9). However, if it rises very much slower than this, steady state is not reached within 20 s, which also contradicts our experimental findings. Second, if the acceleration of PIP_2 synthesis decays too quickly after agonist wash-off, PIP_2 levels would continue to drop, which we also did not observe. Therefore, acceleration of PIP_2 synthesis may decline with a time constant of 10 s or longer. We tested whether the model would work assuming that resting kinase rates are zero. It did not. We found that PIP_2 recovery after Oxo-M application occurs too quickly (green trace in Fig. S9), overshoots, or is insufficient, unless a steady resting value for PI 4-kinase activity is assumed (black trace in Fig. S9). Although we did not include it in the model, the acceleration of PIP_2 synthesis might start faster and last longer as the concentration of Oxo-M is raised. Indeed, the model does not fully reproduce the observed difference in response duration between 0.1 and 10 µM Oxo-M for the DAG and IP_3 reporters, and the time constants derived for 10 µM Oxo-M produce the mentioned transients for other concentrations (see Fig. S4 B of our companion paper). Because these findings suggest that kinase acceleration tracks G_qPCR activation fairly closely, calcium with its transient and more autonomous time course is perhaps not as likely to underlie the acceleration of PIP_2 synthesis as, for example, G protein α or βγ subunits.

At this point, the major unresolved question for the future is how to introduce acceleration of the lipid kinases into the model in a proven mechanistic manner that depends on other components of the model rather than using an empirical ad hoc time course of acceleration. Such a model should include in a natural way any dependence of acceleration on time and on the strength of receptor activation. In addition the complexities of calcium dynamics, clearance, buffering, and SOCE remain to be included.

Conclusion

Our experiments and modeling have shown that apparent qualitative differences in downstream signaling from muscarinic and purinergic G_qPCRs can be understood as entirely caused by differences in receptor density. We also find that a very low threshold for IP_3-dependent calcium release and the cooperative nature of the release kinetics mean that large, nearly regenerative calcium signals are elicited by quite weak stimulation of G_qPCR pathways. Finally, we find that receptor stimulation is accompanied by acceleration of the enzymes of PIP_2 synthesis, but we do not know the underlying mechanism. Our companion paper continues the analysis of DAG production and PKC stimulation and gives further details of our model.

We thank Drs. Jill B. Jensen, Martin Kruse, and Byung-Chang Suh for advice and assistance with molecular biology and commenting on the manuscript; Dr. T. Kendall Harden for discussion of $P2Y_2$Rs; and Lea M. Miller for technical help.

Our work was supported by National Institutes of Health (NIH) grants R01 NS08174 and R01 GM83913, the Human Frontier Science Program, the Interdisciplinary Centre for Clinical Research within the Faculty of Medicine at RWTH Aachen University, and NIH grant RR025429 (to Sharona E. Gordon). The Virtual Cell is supported by NIH grant P41RR013186 from the National Center for Research Resources.

Edward N. Pugh Jr. served as editor.

Submitted: 23 August 2012
Accepted: 21 March 2013

REFERENCES

Atwood, B.K., J. Lopez, J. Wager-Miller, K. Mackie, and A. Straiker. 2011. Expression of G protein-coupled receptors and related proteins in HEK293, AtT20, BV2, and N18 cell lines as revealed by microarray analysis. *BMC Genomics.* 12:14. http://dx.doi.org/10.1186/1471-2164-12-14

Balla, A., Y.J. Kim, P. Varnai, Z. Szentpetery, Z. Knight, K.M. Shokat, and T. Balla. 2008. Maintenance of hormone-sensitive phosphoinositide pools in the plasma membrane requires phosphatidylinositol 4-kinase IIIα. *Mol. Biol. Cell.* 19:711–721. http://dx.doi.org/10.1091/mbc.E07-07-0713

Balla, T. 2007. Imaging and manipulating phosphoinositides in living cells. *J. Physiol.* 582:927–937. http://dx.doi.org/10.1113/jphysiol.2007.132795

Bezprozvanny, I., J. Watras, and B.E. Ehrlich. 1991. Bell-shaped calcium-response curves of Ins(1,4,5)P_3- and calcium-gated channels from endoplasmic reticulum of cerebellum. *Nature.* 351:751–754. http://dx.doi.org/10.1038/351751a0

de Saint-Jean, M., V. Delfosse, D. Douguet, G. Chicanne, B. Payrastre, W. Bourguet, B. Antonny, and G. Drin. 2011. Osh4p exchanges sterols for phosphatidylinositol 4-phosphate between lipid bilayers. *J. Cell Biol.* 195:965–978. http://dx.doi.org/10.1083/jcb.201104062

Delmas, P., and D.A. Brown. 2002. Junctional signaling microdomains: bridging the gap between the neuronal cell surface and Ca^{2+} stores. *Neuron.* 36:787–790. http://dx.doi.org/10.1016/S0896-6273(02)01097-8

Delmas, P., M. Crest, and D.A. Brown. 2004. Functional organization of PLC signaling microdomains in neurons. *Trends Neurosci.* 27:41–47. http://dx.doi.org/10.1016/j.tins.2003.10.013

Dutt, P., L. Kjoller, M. Giel, A. Hall, and D. Toksoz. 2002. Activated $G\alpha_q$ family members induce Rho GTPase activation and Rho-dependent actin filament assembly. *FEBS Lett.* 531:565–569. http://dx.doi.org/10.1016/S0014-5793(02)03625-6

Falkenburger, B.H., J.B. Jensen, and B. Hille. 2010a. Kinetics of M_1 muscarinic receptor and G protein signaling to phospholipase C in living cells. *J. Gen. Physiol.* 135:81–97. http://dx.doi.org/10.1085/jgp.200910344

Falkenburger, B.H., J.B. Jensen, and B. Hille. 2010b. Kinetics of PIP_2 metabolism and KCNQ2/3 channel regulation studied with a voltage-sensitive phosphatase in living cells. *J. Gen. Physiol.* 135:99–114. http://dx.doi.org/10.1085/jgp.200910345

Falkenburger, B.H., E.J. Dickson, and B. Hille. 2013. Quantitative properties and receptor reserve of the DAG and PKC branch of G_q-coupled receptor signaling. *J. Gen. Physiol.* 141:537–555.

Foskett, J.K., C. White, K.H. Cheung, and D.O.D. Mak. 2007. Inositol trisphosphate receptor Ca^{2+} release channels. *Physiol. Rev.* 87:593–658. http://dx.doi.org/10.1152/physrev.00035.2006

Gamper, N., V. Reznikov, Y. Yamada, J. Yang, and M.S. Shapiro. 2004. Phosphatidylinositol 4,5-bisphosphate signals underlie receptor-specific $G_{q/11}$-mediated modulation of N-type Ca^{2+} channels. *J. Neurosci.* 24:10980–10992. http://dx.doi.org/10.1523/JNEUROSCI.3869-04.2004

Horowitz, L.F., W. Hirdes, B.C. Suh, D.W. Hilgemann, K. Mackie, and B. Hille. 2005. Phospholipase C in living cells: Activation, inhibition, Ca^{2+} requirement, and regulation of M current. *J. Gen. Physiol.* 126:243–262. http://dx.doi.org/10.1085/jgp.200509309

Jensen, J.B., J.S. Lyssand, C. Hague, and B. Hille. 2009. Fluorescence changes reveal kinetic steps of muscarinic receptor–mediated modulation of phosphoinositides and Kv7.2/7.3 K^+ channels. *J. Gen. Physiol.* 133:347–359. http://dx.doi.org/10.1085/jgp.200810075

Kanaho, Y., A. Kobayashi-Nakano, and T. Yokozeki. 2007. The phosphoinositide kinase PIP5K that produces the versatile signaling phospholipid PI4,5P_2. *Biol. Pharm. Bull.* 30:1605–1609. http://dx.doi.org/10.1248/bpb.30.1605

Koizumi, S., P. Rosa, G.B. Willars, R.A. Challiss, E. Taverna, M. Francolini, M.D. Bootman, P. Lipp, K. Inoue, J. Roder, and A. Jeromin. 2002. Mechanisms underlying the neuronal calcium sensor-1-evoked enhancement of exocytosis in PC12 cells. *J. Biol. Chem.* 277:30315–30324. http://dx.doi.org/10.1074/jbc.M201132200

Logothetis, D.E., V.I. Petrou, S.K. Adney, and R. Mahajan. 2010. Channelopathies linked to plasma membrane phosphoinositides. *Pflugers Arch.* 460:321–341. http://dx.doi.org/10.1007/s00424-010-0828-y

Matsu-ura, T., T. Michikawa, T. Inoue, A. Miyawaki, M. Yoshida, and K. Mikoshiba. 2006. Cytosolic inositol 1,4,5-trisphosphate dynamics during intracellular calcium oscillations in living cells. *J. Cell Biol.* 173:755–765. http://dx.doi.org/10.1083/jcb.200512141

Murata, Y., and Y. Okamura. 2007. Depolarization activates the phosphoinositide phosphatase Ci-VSP, as detected in Xenopus oocytes coexpressing sensors of PIP_2. *J. Physiol.* 583:875–889. http://dx.doi.org/10.1113/jphysiol.2007.134775

Nakanishi, S., K.J. Catt, and T. Balla. 1995. A wortmannin-sensitive phosphatidylinositol 4-kinase that regulates hormone-sensitive pools of inositolphospholipids. *Proc. Natl. Acad. Sci. USA.* 92:5317–5321. http://dx.doi.org/10.1073/pnas.92.12.5317

Nakatsu, F., J.M. Baskin, J. Chung, L.B. Tanner, G. Shui, S.Y. Lee, M. Pirruccello, M. Hao, N.T. Ingolia, M.R. Wenk, and P. De Camilli. 2012. PtdIns4P synthesis by PI4KIIIα at the plasma membrane and its impact on plasma membrane identity. *J. Cell Biol.* 199: 1003–1016. http://dx.doi.org/10.1083/jcb.201206095

Nikolaev, V.O., M. Bünemann, L. Hein, A. Hannawacker, and M.J. Lohse. 2004. Novel single chain cAMP sensors for receptor-induced signal propagation. *J. Biol. Chem.* 279:37215–37218. http://dx.doi.org/10.1074/jbc.C400302200

Oude Weernink, P.A., M. Schmidt, and K.H. Jakobs. 2004. Regulation and cellular roles of phosphoinositide 5-kinases. *Eur. J. Pharmacol.* 500:87–99. http://dx.doi.org/10.1016/j.ejphar.2004.07.014

Suh, B.C., and B. Hille. 2008. PIP_2 is a necessary cofactor for ion channel function: how and why? *Annu Rev Biophys.* 37:175–195. http://dx.doi.org/10.1146/annurev.biophys.37.032807.125859

Suh, B.C., T. Inoue, T. Meyer, and B. Hille. 2006. Rapid chemically induced changes of PtdIns(4,5)P_2 gate KCNQ ion channels. *Science.* 314:1454–1457. http://dx.doi.org/10.1126/science.1131163

Tanimura, A., T. Morita, A. Nezu, A. Shitara, N. Hashimoto, and Y. Tojyo. 2009. Use of fluorescence resonance energy transfer-based biosensors for the quantitative analysis of inositol 1,4,5-trisphosphate dynamics in calcium oscillations. *J. Biol. Chem.* 284:8910–8917. http://dx.doi.org/10.1074/jbc.M805865200

Tolias, K.F., J.H. Hartwig, H. Ishihara, Y. Shibasaki, L.C. Cantley, and C.L. Carpenter. 2000. Type Iα phosphatidylinositol-4-phosphate 5-kinase mediates Rac-dependent actin assembly. *Curr. Biol.* 10:153–156. http://dx.doi.org/10.1016/S0960-9822(00)00315-8

Unoki, T., S. Matsuda, W. Kakegawa, N.T. Van, K. Kohda, A. Suzuki, Y. Funakoshi, H. Hasegawa, M. Yuzaki, and Y. Kanaho. 2012. NMDA receptor-mediated PIP5K activation to produce PI(4,5)P_2 is essential for AMPA receptor endocytosis during LTD. *Neuron.* 73:135–148. http://dx.doi.org/10.1016/j.neuron.2011.09.034

van der Wal, J., R. Habets, P. Várnai, T. Balla, and K. Jalink. 2001. Monitoring agonist-induced phospholipase C activation in live cells by fluorescence resonance energy transfer. *J. Biol. Chem.* 276:15337–15344. http://dx.doi.org/10.1074/jbc.M007194200

Volpe, P., B.H. Alderson-Lang, and G.A. Nickols. 1990. Regulation of inositol 1,4,5-trisphosphate-induced Ca^{2+} release. I. Effect of Mg^{2+}. *Am. J. Physiol.* 258:C1077–C1085.

Wang, Y., X. Chen, L. Lian, T. Tang, T.J. Stalker, T. Sasaki, Y. Kanaho, L.F. Brass, J.K. Choi, J.H. Hartwig, and C.S. Abrams. 2008. Loss of PIP5KIβ demonstrates that PIP5KI isoform-specific PIP_2 synthesis is required for IP_3 formation. *Proc. Natl. Acad. Sci. USA.* 105:14064–14069. http://dx.doi.org/10.1073/pnas.0804139105

Wang, Y.J., W.H. Li, J. Wang, K. Xu, P. Dong, X. Luo, and H.L. Yin. 2004. Critical role of PIP5KIγ87 in $InsP_3$-mediated Ca^{2+} signaling. *J. Cell Biol.* 167:1005–1010. http://dx.doi.org/10.1083/jcb.200408008

Willars, G.B., S.R. Nahorski, and R.A. Challiss. 1998. Differential regulation of muscarinic acetylcholine receptor-sensitive polyphosphoinositide pools and consequences for signaling in human neuroblastoma cells. *J. Biol. Chem.* 273:5037–5046. http://dx.doi.org/10.1074/jbc.273.9.5037

Xu, C., J. Watras, and L.M. Loew. 2003. Kinetic analysis of receptor-activated phosphoinositide turnover. *J. Cell Biol.* 161:779–791. http://dx.doi.org/10.1083/jcb.200301070

Zaika, O., G.P. Tolstykh, D.B. Jaffe, and M.S. Shapiro. 2007. Inositol triphosphate-mediated Ca^{2+} signals direct purinergic P2Y receptor regulation of neuronal ion channels. *J. Neurosci.* 27:8914–8926. http://dx.doi.org/10.1523/JNEUROSCI.1739-07.2007

Zaika, O., J. Zhang, and M.S. Shapiro. 2011. Combined phosphoinositide and Ca^{2+} signals mediating receptor specificity toward neuronal Ca^{2+} channels. *J. Biol. Chem.* 286:830–841. http://dx.doi.org/10.1074/jbc.M110.166033

Zhao, X., P. Várnai, G. Tuymetova, A. Balla, Z.E. Tóth, C. Oker-Blom, J. Roder, A. Jeromin, and T. Balla. 2001. Interaction of neuronal calcium sensor-1 (NCS-1) with phosphatidylinositol 4-kinase β stimulates lipid kinase activity and affects membrane trafficking in COS-7 cells. *J. Biol. Chem.* 276:40183–40189.